THERMAL APPLICATIONS OF CARBON NANOTUBES IN POLYETHYLENE GLYCOL IN THE PRESENCE OF MAGNETIC FIELD ON ELECTRONIC DEVICES

WINFRED WANDIA MUTETI

I56/CE/20534/2021

A research project submitted in partial fulfilment of the requirements for the award of the degree of Master of Science in applied mathematics in the School of Pure and Applied Sciences of Kenyatta University

JUNE 2025

D**ECLARATION**

I declare that this project is my original work and has not been presented to any other examination body to be examined.

WINFRED WANDIA MUTETI

Signature ……

Date ……

I56/CE/20534/2021

This project has been submitted for examination with our approval as the University Supervisor.

DR. ISAAC CHEPKWONY

Signature ……

Date ……

DEPARTMENT OF MATHEMATICS AND ACTUARIAL SCIENCE

ACKNOWLEDGMENT

I extend my heartfelt gratitude to all those who contributed to this project, with special thanks to the Almighty God. I am very grateful of the selfless support from my loved ones and my spouse, Dennis. I am also grateful for the continuous guidance provided by my supervisor, Dr. Chepkwony.

DEDICATION

To my esteemed lecturers, whose knowledge and guidance have been the compass guiding this journey. Your encouragement fueled my determination.

To my cherished family members, your unwavering support and understanding made this endeavor possible. Your sacrifices did not go unnoticed.

To my colleagues, whose camaraderie and shared enthusiasm created a motivating environment. Your collaboration added immeasurable value to this pursuit.

I extend my heartfelt gratitude to each one of you. May God richly bless you for being the pillars of strength and inspiration throughout this undertaking.

ABSTRACT

In this study, the thermal management of electronic devices, specifically Central Processing Units (CPUs), using carbon nanotubes (CNT) dispersed in polyethylene glycol (PEG-400) under the influence of a magnetic field was studied. The research optimized cooling performance by enhancing efficiency, extending the operating temperature range, and improving the reliability of such systems. The study modeled impingement cooling using a Darcy-Brinkman-Forchheimer approach and considered the effects of viscous dissipation. The governing nonlinear partial differential equations were converted into nonlinear ordinary differential equations (ODEs) by utilizing similarity variables and solved using MATLAB's bvp4c. CNT-PEG-400 nanofluid flowing via a porous metal foam CPU cooler with a fan and a heated CPU surface was simulated. The investigation of key parameters like Hartmann number, Reynolds number, Darcy number, and porosity revealed that increasing the Darcy number significantly enhances heat transfer. The Hartmann number's effect varies with porosity, where stronger magnetic fields are advantageous for highly porous metal foams, ultimately improving cooling efficiency. CNTs increase both the density and viscosity of PEG-400, leading to enhanced heat transfer characteristics, which improve overall cooling performance. These findings contribute to optimizing cooling strategies for CPUs and other electronic devices, especially when using CNT-PEG-400 nanofluids in the presence of magnetic fields.

Table of Contents

LIST OF TABLES

LIST OF FIGURES

SYMBOLS WITH THEIR MEANINGS

ρ is the density

B is the magnetic field

c_E is the form drag coefficient

Da is the Darcy number

$c_p$is the specific heat

f(Y) are the similarity functions

ν denotes the kinematic viscosity of the fluid

H represents the heat sink height

μ stands for the dynamic viscosity

Ha denotes the Hartmann number

$u\ and\ v$ represent the velocities in the x-direction and y-direction, respectively

K denotes the permeability

Ec stands for the Eckert number

L is the length of the heat sink

θ is the dimensionless temperature

P refers to the Pressure

T indicates the temperature

P also represents the Dimensionless pressure

ϑ is the kinematic viscosity

Pr is the Prandtl number

ε signifies the porosity

Re is the Reynolds number

Φ denotes the viscous dissipation term

T_{in} is the temperature at the inlet

T_w denotes the temperature at the wall

x, y are the Cartesian coordinates

k denotes the thermal conductivity of the fluid

X denotes the dimensionless distance from symmetry axis

φ is the nanoparticle volume fraction

Y is the similarity parameter

σ is the electrical conductivity

eff denotes effective

s denotes solid phase

(nf)- nanofluid

(bf)- base fluid

(np)- nanoparticle

CHAPTER ONE

1.0 Introduction

Electronic devices generate heat during operation, and efficient thermal management is necessary for their optimal performance and longevity. Conventional cooling methods for electronic devices, such as air cooling and liquid cooling, have limitations in terms of efficiency and size, particularly for high-power devices. Due to their exceptional thermal conductivity, carbon nanotubes (CNTs) have become a highly promising material for thermal management applications.

Nanofluids containing carbon nanotubes (CNTs) dispersed in a base fluid such as polyethylene glycol (PEG-400) have demonstrated improved thermal properties. These enhanced fluids show potential for use as coolants in electronic devices. Furthermore, in the presence of a magnetic field, CNT-based nanofluids exhibit unique thermal properties due to CNTs alignment along the magnetic field direction. This alignment results in enhanced thermal conductivity that can bring about improved thermal management of electronic devices (Yu et al., 2021).

Electronic devices that can benefit from this technology include, graphics processing units (GPUs), high-power microprocessors (CPUs), field-programmable gate arrays (FPGAs), and other high-performance computing components. These devices typically operate most efficiently within a specific temperature range. For instance, Central Processing Units typically operate most efficiently within a temperature range of 30°C to 70°C, with a maximum safe operating temperature of around 100°C. GPUs can function at higher temperatures of up to 85°C to 100°C, depending on the specific model and manufacturer. Effective thermal management techniques, such as CNT-based nanofluids, can help extend the temperature range at which electronic devices can operate efficiently and safely. On this

study, we focus on heat dissipation on miniature electronic devices like CPUs so as to maintain their operational efficiency and ensure long-term reliability and performance. Thus, the use of CNT in PEG-400 is a promising approach for thermal management of electronic devices in magnetic field's presence, particularly for high-power devices.

1.1Definition of terms

1.1.1 Hartmann Number: This is a dimensionless parameter accustomed to characterize the behavior of electrically conducting fluids, such as conducting nanofluids, in the existence of a magnetic field. It denotes the ratio of electromagnetic forces to viscous forces and helps determine the magnetic field's effect on the flow of the fluid and transfer of heat (Zamir et al., 2024).

1.1.2 Nusselt Number: It is a dimensionless number, which characterizes the efficiency of heat transfer in a fluid flow relative to purely conductive heat transfer. It is the ratio of convective to conductive heat transfer across a boundary such as the surface of a solid or a wall in contact with the fluid (Adio et al., 2025).

1.1.3 Porosity: is a measure of the void or empty space within a material, normally written as a fraction or percentage. It describes how much of a material's volume is taken by empty spaces (pores) compared to its total volume (Vafai, 2023).

1.1.4 Heat Transfer: The process by which thermal energy is passed on from one object or region to another due to a difference in temperature is known as heat transfer. It can take place through conduction (transfer via physical contact), convection (transfer via the movement of liquid), and radiation (transfer via electromagnetic waves) (Adio et al., 2025).

1.1.5 Viscosity: The internal resistance of a fluid to flow is viscosity. It measures the fluid's resistance to shearing forces and is a measure of its thickness or stickiness.

Fluids that have high viscosity flow sluggishly while fluids with low viscosity flow more easily (ACS Omega Team, 2024).

1.1.6 Density: This is the mass per unit volume of a substance. It represents the compactness or concentration of particles in a given space (ACS Omega Team, 2024).

1.1.7 Thermal Conductivity: This is a measure of a substance's capability to conduct heat. It characterizes the rate at which heat energy is transmitted via a substance by conduction**.** Higher thermal conductivity values indicate better heat transfer capabilities, allowing heat to move more efficiently through the material (Punia et al., 2024).

1.1.8 Single-phase Nanofluid: this is a nanofluid where the nanoparticles uniformly disperse in a single phase of the base fluid, resulting in a homogeneous mixture. In other words, both the base fluid and the nanoparticles exist in the same phase, and there is no clear separation between them (Punia et al., 2024).

1.2 Statement of the problem

The efficient thermal management of electronic devices is important for their optimal performance and longevity. Conventional cooling methods have limitations, particularly for high-power devices, and there is a need for more efficient cooling technologies. Carbon nanotubes have shown promise for thermal management as a result of their high thermal conductivity and unique properties. However, the usage of CNT-based nanofluids for thermal applications on electronic devices in the existence of a magnetic field requires further investigation. Therefore, in this research project, I will investigate the use of CNT in PEG-400 for thermal management of CPUs in the presence of a magnetic field, to improve their efficiency, extend their operating temperature range, and improve their reliability.

1.3 Objectives

1.3.1 General objective

To investigate the use of Carbon Nanotubes (CNTs) in polyethylene glycol (PEG-400) for thermal management of electronic devices like Central Processing Units (CPUs) in the presence of a magnetic field, aiming to improve efficiency, extend the operating temperature range, and improve reliability.

1.3.2 Specific objectives

1. To evaluate the effect of CNT-based nanofluids on the viscosity and density of the cooling medium (PEG-400).
2. To investigate the heat transfer performance of CNT-based nanofluids under the influence of a magnetic field.
3. To investigate the relationship between the Hartmann number and porosity on the Nusselt number.

1.4 Justification

Enhancing Thermal Management: Efficient thermal management is crucial for electronic devices such as CPUs to ensure optimal performance, longevity, and reliability. By investigating the use of CNT in PEG-400, the research aims to contribute to the development of advanced cooling technologies that can effectively dissipate heat generated by high-power electronic devices.

CHAPTER TWO

LITERATURE REVIEW

Thermal management plays a crucial role in upholding the optimal performance and longevity of electronic devices like CPUs. Traditional cooling methods often face limitations, especially for high-power devices, necessitating the exploration of more efficient cooling technologies. Carbon nanotubes (CNTs) have gained significant attention due to their exceptional thermal conductivity and unique properties, making them promising candidates for thermal management applications. This literature review gives an overview of relevant studies on the usage of CNT-based nanofluids in thermal applications for electronic devices, particularly in the existence of a magnetic field.

Some studies have investigated the behavior of nanofluids under the influence of a magnetic field. Sudhakar and Ravi Kumar (2014) observed that the presence of a magnetic field altered the thermal and rheological properties of nanofluids, leading to improved heat transfer characteristics. Dhinesh Kumar and Suresh (2021) focused on the magnetic field-induced thermal convection of nanofluids in geothermal applications, highlighting the potential for enhanced heat transfer performance. These studies emphasize the importance of understanding the interactions between magnetic fields and nanofluids for efficient thermal management.

Studies by Younes et al. (2022) have underscored the importance of understanding key factors affecting their thermal conductivity, such as nanoparticle size, shape, and alignment. Despite extensive research, commercial applications of nanofluids remain limited due to conflicting data on these factors' effects. Parameters like viscosity and stability also pose challenges for wider adoption. This is relevant to my study, which focuses on optimizing the thermal behavior of CNT-PEG nanofluids for enhanced CPU cooling.

Furthermore, Jang et al. (2009) explored CNTs alignment using magnetic fields and aqueous dispersion. They revealed that applying a magnetic field facilitated the alignment of nanotubes, leading to enhanced thermal and mechanical properties.

Open-cell metal foams have many applications (Pourrahmani et al., 2019) and possess excellent thermal properties, making them an ideal candidate for next-generation heat exchangers used in CPU cooling systems (Zing et al., 2019). Additionally, the rapid advancements in nanofluids have garnered significant attention, particularly for incorporating nano-sized metal particles into cooling fluids to enhance heat dissipation (Mahian et al., 2019). Whelan et al., (2012) developed and evaluated a liquid cooling system utilizing nanofluids for an Intel Pentium 4 processor. Their results indicated that a compact nanofluid jet could efficiently dissipate up to 200 W of heat, significantly lowering the overall system cost. Consequently, continued research on the heat transfer properties of nanofluid flow through porous metals is crucial.

Other studies have also contributed significantly to the understanding of CNT-based nanofluids under magnetic fields. Xie et al. (2018) investigated the viscosity of carbon nanotube aqueous nanofluids and found that the application of a magnetic field led to a notable increase in viscosity, attributed to the alignment and clustering of CNTs along magnetic field lines. Cwynar et al. (2020) examined the isobaric heat capacity of CNT-based nanofluids and reported that the presence of a magnetic field enhanced the specific heat capacity, improving the fluid's ability to store and transport thermal energy. Wang et al. (2019) conducted experimental studies on the heat transfer behavior of CNT nanofluids under magnetic influence and observed that the magnetic field significantly improved convective heat transfer by promoting nanoparticle alignment and modifying the flow structure.

Recent studies have increasingly focused on the dynamics of nanofluid heat transfer within porous media. Nabwey et al. (2023) comprehensively reviewed nanofluid behaviors in porous structures, highlighting how key parameters—such as Darcy's number and porosity—substantially affect convective heat transfer performance in Darcy–Brinkman–Forchheimer flows. Their analysis underscores that increasing porous medium permeability (higher Darcy number) directly enhances thermal transport, while porosity variations can either boost or diminish heat exchange depending on geometry and flow conditions. This review establishes a rigorous foundation for understanding parameter sensitivity in porous MHD-enhanced cooling systems.

Building on this framework, a numerical investigation by Abdelaziz et al. (2024) examined forced convective MHD nanofluid flow through pipe geometries containing porous media, utilizing the Darcy–Brinkman–Forchheimer model. Their findings revealed that applying a magnetic field enhances heat-transfer rates, though at the cost of increased pressure drop. Furthermore, the choice of nanoparticle and porous matrix materials critically influenced thermal performance; for instance, aluminum-based nanofluids within silver-porous media demonstrated optimal enhancement according to performance evaluation criteria. These results align closely with experimental trends and support the effective integration of magnetic fields and material selection in optimizing nanofluid cooling systems.

In summary, the reviewed literature demonstrates the potential of CNT-based nanofluids for efficient thermal management in electronic devices particularly, CPUs. The existence of a magnetic field can affect the thermal and rheological properties of nanofluids, leading to improved heat transfer performance. The addition of carbon nanotubes in nanofluids has shown enhancements in thermal conductivity, viscosity, and stability. The studies discussed here provide valuable insights into the behavior of CNT-based nanofluids under the influence

of magnetic fields, highlighting their potential for enhancing the thermal management of electronic devices.

CHAPTER THREE

METHODOLOGY

3.0 Introduction

The current investigation employs a modeling framework based on a CPU cooling system using CNT in PEG-400 nanofluid as in figure 3.0.1.

Figure 3.0.1 CPU cooling system model(Venkateswarlu et al., 2024)

The CPU is modeled as having a metal foam heat sink, which is responsible for dissipating heat. However, the CPU's and heat sink's thermal resistance is neglected. Due to the low Reynolds number, the flow field within the porous media is assumed to be laminar. The physical properties of the CNT-PEG-400 nanofluid are assumed to be constant and not affected by changes in temperature, and a uniform constant magnetic field is applied to the heat sink.

The heat sink's physical properties are assumed to be isotropic and homogeneous with no temperature variability. Due to high flow resistance in the porous medium, I have considered

heat generated by both the friction between the CNT-PEG-400 and the solid pores and viscous dissipation.

3.1 Assumptions

- The nanofluid is assumed to be incompressible and steady
- The viscosity of the nanofluid is consistent and unaffected by shear rate.
- Nanofluid's thermal conductivity is uniform in all directions.
- The metal foam maintains consistent porosity, allowing fluid to flow uniformly through the pores in all directions.
- The magnetic field's intensity and orientation are consistent throughout the study area.
- In the investigation of the porous media, both viscous and inertial forces are taken into consideration.
- Heat is uniformly distributed across the CPU's surface, with no heat transfer occurring through the model's side walls.
- At the porous medium's wall, the flow velocity of the nanofluid is zero.

3.2 Mathematical modelling

The problem is modelled by assuming that in the process of heat dissipation, the drop in pressure and transfer of heat is assumed to be constant, when exposed to a uniformly applied jet velocity. This flow is assumed to be like the flow that occurs between parallel plates as in figure 3.2.1. The flow is parallel to the x-axis, with a uniform velocity distribution along the y-axis, while the heat is being generated. The cooling nanofluid exits the fan with a constant velocity, U_{in}, and temperature, T_{in}. It subsequently enters the heat sink uniformly. Since the CPU's surface is expected to maintain a fixed temperature, we assume the surface maintains a constant temperature, T_w. A magnetic field which is uniform is applied to the porous medium. As the nanofluid flows through the porous metal foam, it effectively transfers the heat generated by the CPU surface to the heat sink boundary. To simplify the analysis, the

symmetry of the physical setup has been utilized. As the system and boundary conditions are symmetric about the centerline, only one half of the geometry is modeled. This approach accurately represents the behavior over the entire CPU surface while reducing computational complexity. Figure 3.2.1 and 3.2.2 shows the porous metal CPU cooler being studied, showing both a 3D view and a 2D model with the corresponding boundary conditions.

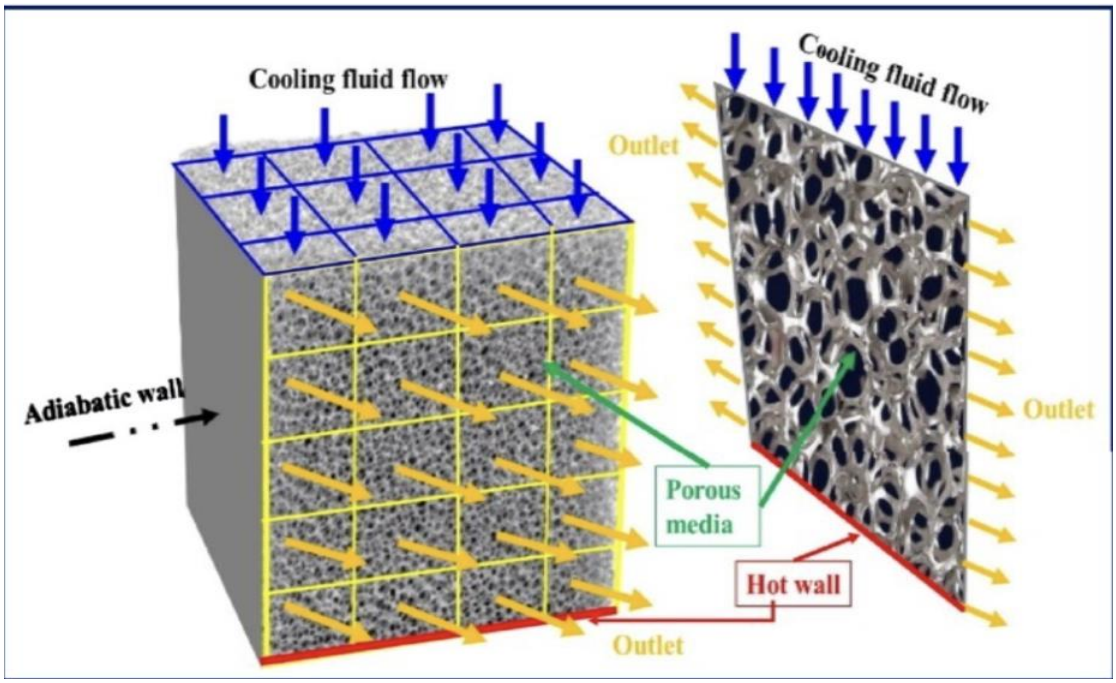

Figure 3.2.1. 3D model of CPU cooler made of porous metal(Venkateswarlu et al., 2024)

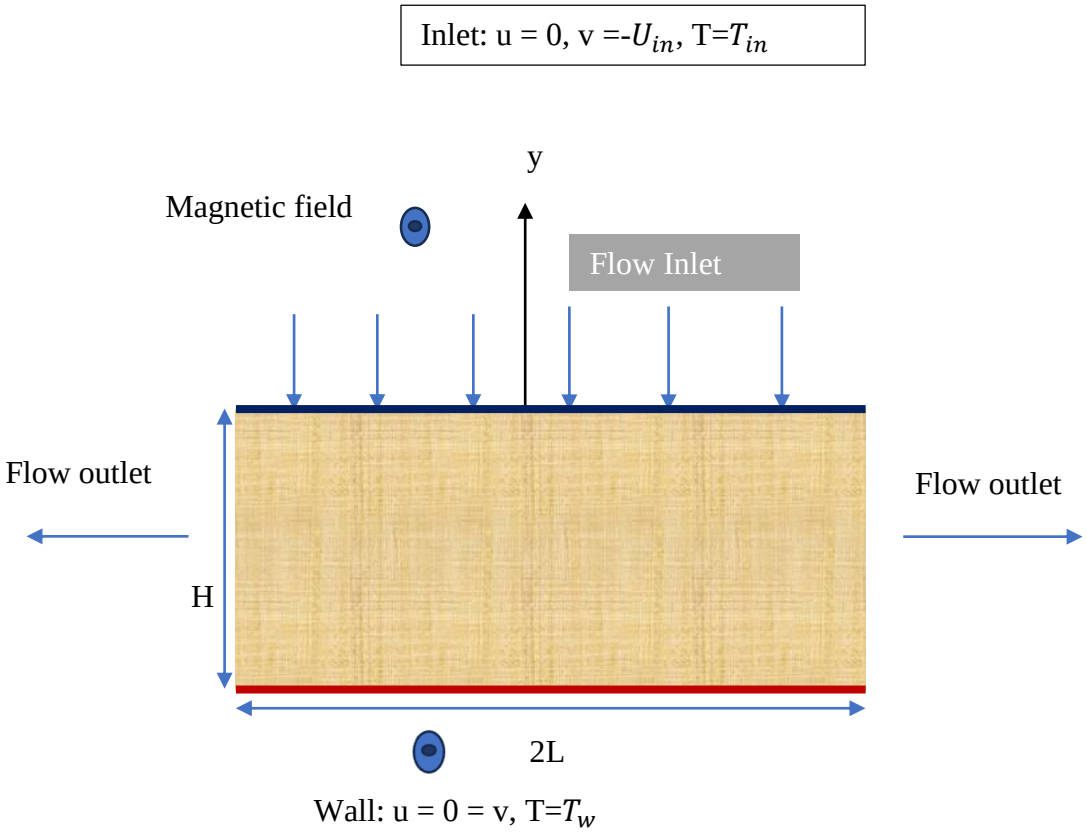

Figure 3.2.2 2D model with the boundary conditions of the CPU cooler

The CNT-PEG-400 nanofluid is assumed to enter the porous media with an unvarying velocity and temperature. The CPU surface is maintained at an unchanging temperature. This ensures that the safe operating temperature range of the CPU is maintained to enhance efficiency, and improve their longevity.

The fundamental equations governing flow and heat transfer are based on the Navier-Stokes equations, which describe the conservation of mass, momentum, and energy. Here is a model of these equations.

3.3 Fundamental equations:

3.3.1 Continuity equation:

This equation denotes the conservation of mass for an incompressible flow. In my study, this equation states that the nanofluid's mass remains constant as it flows through the porous metal foam, even when subjected to a magnetic field.

$$\nabla.(\rho v) = 0 \qquad (3.3.1.1)$$

Since the flow is 2D and incompressible, the equation reduces to:

$$\frac{\partial u}{\partial x} + \frac{\partial v}{\partial y} = 0 \qquad (3.3.1.2)$$

In this context, u and v represent the velocity components along the x-axis and y-axis, respectively.

3.3.2 Momentum equation:

This equation defines fluid substances' motion. The equation is essential for determining the flow behaviour of the nanofluid subject to a magnetic field, which affects how the fluid distributes the heat generated by the CPU and is given by:

$$\rho(\upsilon.\nabla)\upsilon = -\nabla p + \mu\nabla^2\upsilon + F \qquad (3.3.2.1)$$

Where:

υ represents the velocity

ρ denotes the fluid density

p stands for the pressure

F indicates the body forces per unit volume.

μ is the dynamic viscosity

x-momentum:

$$\frac{1}{\varepsilon^2}\left(u\frac{\partial u}{\partial x} + v\frac{\partial u}{\partial y}\right) = -\frac{1}{\rho_{nf}}\frac{\partial p}{\partial x} + \frac{\vartheta_{nf}}{\varepsilon}\left(\frac{\partial^2 u}{\partial x^2} + \frac{\partial^2 u}{\partial y^2}\right) - \left(\frac{\sigma_{nf}}{\rho_{nf}}B_0^2 + \frac{\vartheta_{nf}}{K^*} + \frac{C_E}{\sqrt{k^*}}\sqrt{u^2+v^2}\right)u \qquad (3.3.2.2)$$

y-momentum:

$$\frac{1}{\varepsilon^2}\left(u\frac{\partial v}{\partial x}+v\frac{\partial v}{\partial y}\right)=-\frac{1}{\rho_{nf}}\frac{\partial p}{\partial y}+\frac{\vartheta_{nf}}{\varepsilon}\left(\frac{\partial^2 v}{\partial x^2}+\frac{\partial^2 v}{\partial y^2}\right)-\left(\frac{\sigma_{nf}}{\rho_{nf}}B_0^2+\frac{\vartheta_{nf}}{K^*}+\frac{C_E}{\sqrt{k^*}}\sqrt{u^2+v^2}\right)v \quad (3.3.2.3)$$

Where:

ε is medium's porosity

k^* stands for the thermal conductivity

T represents the temperature

σ_{nf} denotes the electrical conductivity of the nanofluid

K^* signifies the permeability of the porous medium.

ρ_{nf} stands for the density of the nanofluid

$C_E$is the coefficient of form drag

ϑ_{nf} indicates the kinematic viscosity of the nanofluid

B_0 is the magnetic field strength that is applied

σ_{nf} is the electrical conductivity of the nanofluid.

$\frac{\vartheta_{nf}}{K^*}u$ represents the Darcy term.

$\left(\frac{C_E}{\sqrt{k^*}}\sqrt{u^2+v^2}\right)u$ represents the Forchheimer term.

The Lorentz force, resulting from the interaction between the magnetic field and the moving nanofluid, is represented by the term $\frac{\sigma_{nf}}{\rho_{nf}}B_0^2$

$\frac{C_E}{\sqrt{k^*}}$ accounts for the drag force within the porous medium

3.3.3 Energy equation

This equation accounts for energy conservation (heat transfer) in the nanofluid. The energy equation is important because it accounts for the temperature variations caused by heat generation, especially subject to a magnetic field. The formula for energy can be expressed as follows:

$$u\frac{\partial T}{\partial x}+v\frac{\partial T}{\partial y}=\frac{k_{eff}}{(\rho C_p)_{nf}}\left(\frac{\partial^2 T}{\partial x^2}+\frac{\partial^2 T}{\partial y^2}\right)+\frac{Q^*}{(\rho C_p)_{nf}}(T-T_{in})+\Phi \quad (3.3.3.1)$$

Where:

$$\Phi = \frac{\mu_{nf}}{K^*}(u^2 + v^2) + \frac{\mu_{nf}}{\varepsilon}\left\{2\left(\frac{\partial u}{\partial x}\right)^2 + \left(\frac{\partial v}{\partial y}\right)^2 + \left(\frac{\partial v}{\partial x} + \frac{\partial u}{\partial y}\right)^2\right\} \quad (3.3.3.2)$$

k_{eff} is the effective thermal conductivity

$(\rho)_{nf}$ is the density for the nanofluid.

The specific heat capacity of the nanofluid is denoted as $(C_p)_{nf}$

Φ represents the viscous dissipation effects.

3.4 Boundary Conditions

Inlet boundary: Located at y = H, where the nanofluid enters the channel:

u = 0, v = $-U_{in}$, T= T_{in} (3.4.1)

Wall: Located at y = 0 (no-slip wall):

u = 0 = v, T= T_w (3.4.2)

3.5 Nanofluid thermophysical properties

Table 3.5.0.1 properties of the nanoparticles and base fluid (Yin et al., 2008, Narang & Pundir, 2018, Marcos et al., 2019)

	$\boldsymbol{\rho(kg/m^3)}$	$\boldsymbol{C_p(J/Kg.K)}$	$\boldsymbol{k(W/m.K)}$	$\boldsymbol{\sigma(\Omega m)^{-1}}$
PEG-400	1125	2400	0.186	10^{-8}
CNTs	1400	700	4000	10^{8}

Table 3.5.0.2 properties of the Metal foam (Calmidi et al., 2000)

	Porosity	$\boldsymbol{c_E}$	**K(x$10^7 m^2$)**	$\boldsymbol{k_s(W/m.K)}$
Metal foam	0.9118	0.085	1.8	95

The thermophysical properties of the CNT-PEG-400 nanofluid, which include viscosity, density, and effective thermal conductivity, can be computed by use of the following classical models:

3.5.1 Viscosity

I utilized the Brinkman equation to determine how carbon nanotubes (CNTs) influence the viscosity of polyethylene glycol (PEG-400).This equation defines the nature of the fluid motion via packed layers (Marcos et al., 2019). The equation is given by:

$$\mu_{nf} = \frac{\mu_{bf}}{(1-\phi)^{2.5}} \qquad (3.5.1.1)$$

ϕ is the nanofluid's concentration

The subscripts 'nf' and 'bf' denote the nanofluid and base fluid, respectively.

Given:

- Volume fraction of CNTs (ϕ) = 5% = 0.05
- Viscosity of base fluid (μ_{bf}) = 90 cP = 90 mPa.s

Substituting these values we get:

$$\mu_{nf} = 102.31 mPa.s$$

The viscosity of the nanofluid increases slightly in comparison with the viscosity of the base fluid due to the addition of CNTs.

3.5.2 Density

To calculate the effect of CNT-based nanofluids on the density of the PEG-400, I have used the rule of mixtures. The rule of mixtures is a method used to predict different properties of a composite material. The mixture model for calculating the density of the CNT-PEG-400 mixture is based on the weighted sum of the densities of the individual components. This approach is commonly used in the study of nanofluids and mixtures (Sarkar, 2019; Li et al., 2020).

This model assumes ideal mixing of the components in the mixture and neglects any interactions between CNTs and PEG-400 that may affect the overall density. The mixture model assumes that the nanofluid can be treated as a homogeneous mixture, where the overall density ρ_{nf} is a weighted average of the densities of the individual components. The equation is given by:

$$\rho_{nf} = \rho_{np}\phi + \rho_{bf}(1 - \phi) \quad (3.5.2.1)$$

Where:

ρ_{nf} is the nanofluid's density,

ϕ is the concentration of CNTs in the nanofluid,

ρ_{bf} represents the base fluid's density.

ρ_{np} denotes the density of the nanoparticles.

After reviewing existing literature related to CNT-based nanofluids, I found valuable insights into typical volume fractions and densities of CNT used in research. In the study by Li et al. (2018), they synthesized CNTs and the density of the resulting carbon nanotubes was found to be approximately 1.8 g/cm³. According to the review article by Ahmadi et al. (2018), volume fractions of carbon nanotubes (CNTs) in nanofluids for cooling applications typically range from 0.1% to 5%. In my research, I am using the volume fraction of 5%.

According to the Material Safety Data Sheet (MSDS) provided by Sigma-Aldrich for polyethylene glycol 400 (PEG-400), the density of PEG-400 at room temperature (approximately 25°C) is approximately 1.128 grams per cubic centimeter (g/cm³). Replacing the above parameters into the mixture's equation:

Given:

- Volume fraction of CNTs (ϕ) = 1% = 0.05
- Density of CNTs (ρ_{np}) = 1.8 g/cm³
- Density of base fluid (ρ_{bf}) = 1.128 g/cm³

$$\rho_{nf} = \rho_{np}\phi + \rho_{bf}(1-\phi)$$

$$\rho_{nf} = (1.8\ \mathrm{g/cm^3})(0.05) + (1.128\ \mathrm{g/cm^3})(1-0.05)$$

$$\rho_{nf} = 1.1616\ \mathrm{g/cm^3}$$

Therefore, the density of the CNT-based nanofluid in PEG-400 is approximately $1.1616\ \mathrm{g/cm^3}$.

3.5.3 Effective thermal conductivity

$$k_{eff} = \varepsilon k_{nf} + (1-\varepsilon)k_s \qquad (3.5.3.1)$$

Where

$$\frac{k_{nf}}{k_{bf}} = \frac{k_{np} + 2k_{bf} - 2\phi(k_{bf} - k_{np})}{k_{np} + 2k_{bf} + \phi(k_{bf} - k_{np})}$$

The porous medium has a solid phase thermal conductivity of 95 W/m.K and a porosity of 0.9. To determine the effective thermal conductivity of the nanofluid, the following substitutions are made in the given equation:

k_{bf} = 0.186 W/m.K

k_{np}= 4000 W/m.K

ϕ = 0.05

By substituting these values into the aforementioned equation, the effective thermal conductivity of the CNT-PEG-400 nanofluid is calculated to be 0.2154 W/m.K. Consequently, the effective thermal conductivity is determined to be 9.69386 W/m.K.

3.6 Normalization of governing equations

To nondimensionalize the above equations, the following dimensionless variables are used:

$$U = \frac{u}{U_{in}}, V = \frac{v}{U_{in}}, P = \frac{p}{\rho_{nf}U_{in}^2}, X = \frac{x}{H}, Y = \frac{y}{H}, \theta = \frac{T-T_{in}}{T_w - T_{in}} \qquad (3.6.1)$$

Starting with the continuity equation and using the dimensionless variables above, we get:

$$\frac{\partial u}{\partial x}+\frac{\partial v}{\partial y}=0 \qquad (3.6.2)$$

Substituting for u, x, and y, we get:

$$\frac{U_{in}}{H}\frac{\partial U}{\partial X}+\frac{U_{in}}{H}\frac{\partial V}{\partial Y}=0 \qquad (3.6.3)$$

Which simplifies to:

$$\frac{\partial U}{\partial X}+\frac{\partial V}{\partial Y}=0 \qquad (3.6.4)$$

Doing the same for the momentum equations and using the Darcy number (Da_H), Eckert number (Ec), heat source (Q), Reynolds number (Re_H), Hartmann number (Ha_H), Prandtl number (Pr), convection (λ_H), and distance from the symmetric axis (X), dimensionless parameters expressed as:

$$Da_H=\frac{K}{H^2}=(\frac{L}{H})^2\frac{K}{L^2}=(\frac{H}{L})^{-2}Da_L, \qquad Ec=\frac{U_{in}^2}{(Cp)_{nf}(T_w-T_{in})}, \qquad Q=\frac{Q^*H^2}{\vartheta_{nf}(\rho Cp)_{nf}},$$

$$Re_H=\frac{HU_{in}}{\vartheta_{nf}}=\left(\frac{H}{L}\right)\frac{LU_{in}}{\vartheta_{nf}}=\left(\frac{H}{L}\right)Re_L,$$

$$Ha_H=HB\sqrt{\frac{\sigma_{nf}}{\mu_{nf}}}=\left(\frac{H}{L}\right)LB\sqrt{\frac{\sigma_{nf}}{\mu_{nf}}}=\left(\frac{H}{L}\right)Ha_L, \qquad Pr=\frac{\vartheta_{nf}(\rho Cp)_{nf}}{k_{nf}},$$

$$\lambda=\frac{Gr}{Re_H}, \qquad X=\frac{x}{H}=\left(\frac{L}{H}\right)\frac{x}{L}=(\frac{H}{L})^{-1}X_L, \qquad Gr=\frac{g\beta_{nf}H}{U_{in}^2}(T_w-T_{in})$$

we get:

x-momentum:

$$\frac{1}{\varepsilon^2}\left(u\frac{\partial u}{\partial x}+v\frac{\partial u}{\partial y}\right)=-\frac{1}{\rho_{nf}}\frac{\partial p}{\partial x}+\frac{\vartheta_{nf}}{\varepsilon}\left(\frac{\partial^2 u}{\partial x^2}+\frac{\partial^2 u}{\partial y^2}\right)-\left(\frac{\sigma_{nf}}{\rho_{nf}}B_0^2+\frac{\vartheta_{nf}}{K^*}+\frac{C_E}{\sqrt{k^*}}\sqrt{u^2+v^2}\right)u$$

y-momentum:

$$\frac{1}{\varepsilon^2}\left(u\frac{\partial v}{\partial x}+v\frac{\partial v}{\partial y}\right)=-\frac{1}{\rho_{nf}}\frac{\partial p}{\partial y}+\frac{\vartheta_{nf}}{\varepsilon}\left(\frac{\partial^2 v}{\partial x^2}+\frac{\partial^2 v}{\partial y^2}\right)-\left(\frac{\vartheta_{nf}}{K^*}+\frac{C_E}{\sqrt{k^*}}\sqrt{u^2+v^2}\right)v$$

The x-momentum equation becomes:

$$\frac{1}{\varepsilon^2}\left(U\frac{\partial U}{\partial X}+V\frac{\partial U}{\partial Y}\right)=-\frac{\partial P}{\partial X}+\frac{1}{\varepsilon Re_H}\left(\frac{\partial^2 U}{\partial X^2}+\frac{\partial^2 U}{\partial Y^2}\right)-\frac{1}{Re_H Da_H}U-$$

$$\frac{c_E}{\sqrt{Da_H}}\left(\sqrt{U^2+V^2}\right)U-\frac{Ha_H^2}{Re_H}U \tag{3.6.5}$$

And the y-momentum becomes:

$$\frac{1}{\varepsilon^2}\left(U\frac{\partial V}{\partial X}+V\frac{\partial V}{\partial Y}\right)=-\frac{\partial P}{\partial Y}+\frac{1}{\varepsilon Re_H}\left(\frac{\partial^2 V}{\partial X^2}+\frac{\partial^2 V}{\partial Y^2}\right)-\frac{1}{Re_H Da_H}V-\frac{c_E}{\sqrt{Da_H}}\left(\sqrt{U^2+V^2}\right)V \tag{3.6.6}$$

The energy equation becomes:

$$PrRe_H\left(U\frac{\partial \theta}{\partial X}+V\frac{\partial \theta}{\partial Y}\right)=\left(\frac{\partial^2 \theta}{\partial X^2}+\frac{\partial^2 \theta}{\partial Y^2}\right)+PrEc\left\{\frac{1}{Da_H}(U^2+V^2)+\frac{1}{\varepsilon}\left(2\left[\left(\frac{\partial U}{\partial X}\right)^2+\left(\frac{\partial V}{\partial Y}\right)^2\right]+\left[\frac{\partial U}{\partial Y}+\frac{\partial V}{\partial X}\right]^2\right)\right\} \tag{3.6.7}$$

3.7 Similarity Solution

The similarity solution is employed to reduce the partial differential equations (PDEs) to ordinary differential equations (ODEs) by introducing a similarity variable that combines the independent variables into a single variable. According to the research done by Feng et al., 2015, equations (3.6.4) to (3.6.6) can be formulated as:

$$\frac{\partial U}{\partial X}+\frac{\partial V}{\partial Y}=0 \tag{3.7.1}$$

$$\frac{1}{\varepsilon^2}\left(U\frac{\partial U}{\partial X}+V\frac{\partial U}{\partial Y}\right)=-\frac{\partial P}{\partial X}+\frac{1}{\varepsilon Re_H}\left(\frac{\partial^2 U}{\partial X^2}+\frac{\partial^2 U}{\partial Y^2}\right)-\frac{1}{Re_H Da_H}U-$$

$$\frac{c_E}{\sqrt{Da_H}}|U|U-\frac{Ha_H^2}{Re_H}U \tag{3.7.2}$$

$$\frac{1}{\varepsilon^2}\left(U\frac{\partial V}{\partial X}+V\frac{\partial V}{\partial Y}\right)=-\frac{\partial P}{\partial Y}+\frac{1}{\varepsilon Re_H}\left(\frac{\partial^2 V}{\partial X^2}+\frac{\partial^2 V}{\partial Y^2}\right)-\frac{1}{Re_H Da_H}V-\frac{c_E}{\sqrt{Da_H}}|V|V \tag{3.7.3}$$

We can then use the following similarity parameters

$$U=Xf'(Y),\ V=-f(Y),\ \theta=\theta(Y) \tag{3.7.4}$$

Substituting the transformations, (3.7.2) & (3.7.3) become:

$$\frac{\partial P}{\partial X} = X\left(\frac{1}{\varepsilon^2}(ff'' - f'^2) + \frac{1}{\varepsilon Re_H}f''' - \frac{1}{Re_H}\left(\frac{1}{Da_H} + Ha_H^2\right)f - \frac{c_E}{\sqrt{Da_H}}Xf'^2\right) \quad (3.7.5)$$

$$\frac{\partial P}{\partial Y} = \frac{1}{Re_H Da_H}f + \frac{c_E}{\sqrt{Da_H}}f^2 - \frac{1}{\varepsilon Re_H}f'' - \frac{1}{\varepsilon^2}ff' \quad (3.7.6)$$

Eliminating the pressure gradient, we get a 4th order non-linear ode:

$$f^{iv} + \frac{Re_H}{\varepsilon}ff''' - \left(2c_E\varepsilon X\frac{Re_H}{\sqrt{Da_H}} + \frac{Re_H}{\varepsilon}\right)f'f'' - \varepsilon\left(\frac{1}{Da_H} + Ha_H^2\right)f'' = 0 \quad (3.7.7)$$

Considering the following boundary conditions:

$$f(0) = 0, f'(0) = 0, f(1) = 1, f'(1) = 0 \quad (3.7.8)$$

The energy equation can also be transformed to the following, by employing the similarity analysis:

$$\theta'' + PrRe_H f\theta' + PrEc\left\{\frac{1}{Da_H}(X^2f'^2 + f^2) + \frac{1}{\varepsilon}(4f'^2 + X^2f''^2)\right\} = 0 \quad (3.7.9)$$

With the B.Cs:

$$\theta(0) = 1, \theta(1) = 0 \quad (3.7.10)$$

To analyze the heat transfer efficiency of CNT-PEG-400, the Nusselt number will be calculated using the following equations:

$$Nu = \frac{hL}{k_{bf}}\ where: h = \frac{q''_{wall}}{\Delta T}\ and\ q''_{wall} = -k_{eff}\left(\frac{\partial T}{\partial y}|_{y=0} = -k_{eff}\frac{\Delta T}{H}\theta'(0)\right) \quad (3.7.11)$$

$$=> Nu = -\frac{k_{eff}}{k_{bf}}\left(\frac{H}{L}\right)^{-1}\theta'(0) \quad (3.7.12)$$

3.8 Validation

The similarity solution for flow and forced convective heat transfer was numerically solved using the finite difference method implemented through MATLAB's *bvp4c* solver (Shampine et al., 2003) under specific boundary conditions. The solution's accuracy was confirmed by comparing it with both experimental and analytical data from Do et al.'s study. The findings demonstrated a strong agreement between the analytical predictions and the experimental outcomes.

CHAPTER FOUR

NUMERICAL METHOD, RESULTS AND DISCUSSIONS

4.0 Introduction

The derived similarity solution was employed to explore the impact of different dimensionless parameters on fluid flow and heat transfer characteristics. This investigation specifically analyzed velocity, temperature, and Nusselt number profiles. The study concentrated on significant dimensionless numbers, including the Reynolds number, Darcy number, Hartmann number, and porosity. The reference values for these parameters are provided in Table (4.0.1). Importantly, to maintain consistency in the analysis, when one dimensionless parameter was varied, the others were kept constant.

Table 4.0.1 reference values for different dimensionless numbers

H/L	c_E	ε	X	ϕ	Da_H	Ha_H	Ec_H
1	0.09	0.9	1	0.05	5×10^{-3}	20	0.001

4.1 Momentum equation:

To solve the 4th order momentum equation, I have introduced new variables to break the equation into a system of 1st order ODEs.

$$f^{iv} + \frac{Re_H}{\varepsilon} f f''' - \left(2c_E \varepsilon X \frac{Re_H}{\sqrt{Da_H}} + \frac{Re_H}{\varepsilon} \right) f' f'' - \varepsilon \left(\frac{1}{Da_H} + Ha_H^2 \right) f'' = 0$$

We are going to let:

$$y_1 = f,\ y_2 = f',\ y_3 = f'',\ y_4 = f''' \qquad (4.1.1)$$

Then the system becomes:

$$\left.\begin{aligned} y_1' &= y_2 \\ y_2' &= y_3 \\ y_3' &= y_4 \\ y_4' &= -\frac{Re_H}{\varepsilon} y_1 y_4 + \left(2c_E \varepsilon X \frac{Re_H}{\sqrt{Da_H}} + \frac{Re_H}{\varepsilon}\right) y_2 y_3 + \varepsilon \left(\frac{1}{Da_H} + Ha_H^2\right) y_3 \end{aligned}\right\} \quad (4.1.2)$$

The BCs become:

$$y_1(0) = 0,\ y_2(0) = 0,\ y_1(1) = 1,\ y_2(1) = 0 \quad (4.1.3)$$

Equation (4.1.2) was subsequently solved numerically using MATLAB's *bvp4c* solver, which applies a collocation-based finite difference method for boundary value problems.

4.2 Energy equation

$$\theta'' + PrRe_H f\theta' + PrEc\left\{\frac{1}{Da_H}(X^2 f'^2 + f^2) + \frac{1}{\varepsilon}(4f'^2 + X^2 f''^2)\right\} = 0$$

To transform the energy equation into a system of first-order ordinary differential equations (ODEs), we define:

$$y_1 = \theta,\ y_2 = \theta' \quad (4.2.1)$$

Then, the system becomes:

$$\left.\begin{aligned} y_1' &= y_2 \\ y_2' &= -PrRe_H f y_2 - PrEc\left(\frac{1}{Da_H}(X^2 f'^2 + f^2) + \frac{1}{\varepsilon}(4f'^2 + X^2 f''^2)\right) \end{aligned}\right\} \quad (4.2.2)$$

4.3 RESULTS AND DISCUSSION

4.3.1 Effect on density

Based on the rule of mixtures, the base fluid has a density of 1.128 g/cm³, while the nanofluid's density is calculated to be 1.1616 g/cm³. This indicates that the addition of CNTs results in a slight increase in the density of the Polyethylene Glycol base fluid.

The increase in density may have implications for various applications of CNT-based nanofluids, such as thermal management. Increased mixture density results in better thermal performance, enabling electronic devices to operate at lower temperatures. This is particularly crucial for high-power electronic components, where effective cooling is essential to maintain optimal performance and reliability.

4.3.2 Effect on viscosity

After calculating the effect on viscosity using the Brinkman equation, the viscosity of the nanofluid was $102.31 mPa.s$ while that of the base fluid was $90 mPa.s$. The viscosity of the CNT-PEG-400 nanofluid increases compared to the viscosity of the base fluid due to the addition of CNTs. While the increase in viscosity of a CNT-based nanofluid in PEG-400 can enhance heat transfer performance, it also poses challenges such as higher energy consumption and pressure drop. Balancing these factors is critical in optimizing thermal management systems for efficient cooling while ensuring stability and reliability.

4.4 Investigation of heat transfer performance

4.4.1 Darcy number study

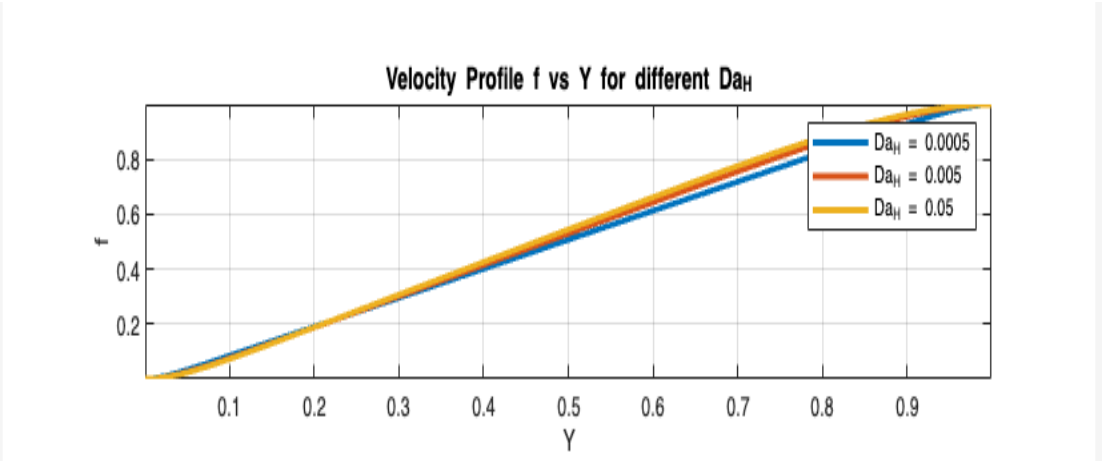

Figure 4.4.1.1 variation of f with respect to Da_H

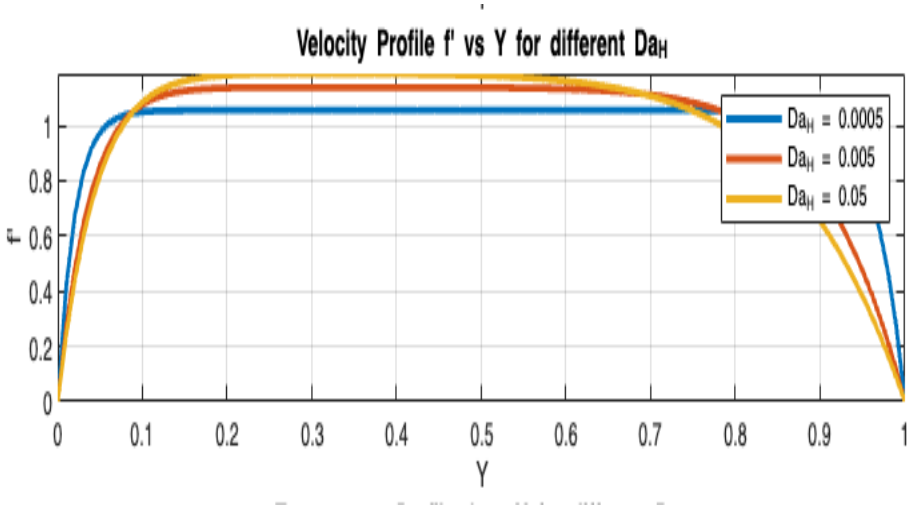

Figure 4.4.1.2 variation of f' with respect to Da_H

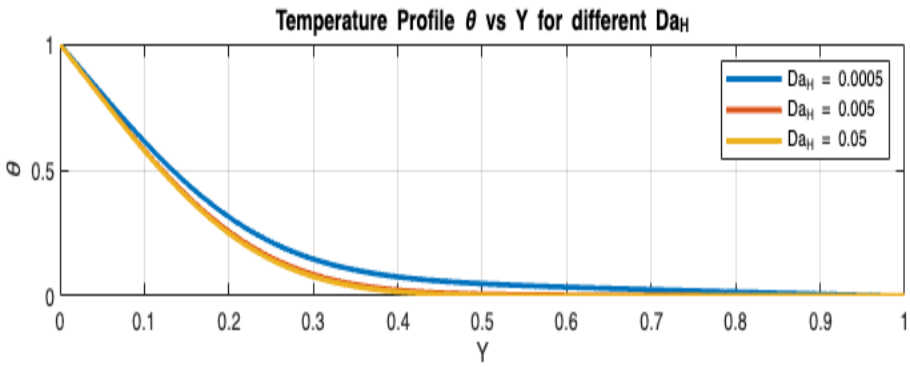

figure 4.4.1.3 variation of θ with respect to Da_H

Figures 4.4.1.1, 4.4.1.2 and 4.4.1.3 illustrates the changes in the distributions of (f), (f'), and (θ) in relation to (Da_H) respectively. According to Equation (3.7.4), (f) and (f') represent the non-dimensional velocity components in the y-direction and x-direction, respectively. As illustrated in Figure 4.4.1.1, the function (f) exhibits an almost linear increase with (Y). This trend signifies a shift in velocity from a purely vertical flow to a point of zero velocity as the fluid ascends from the fan positioned above the porous medium to the heated surface. With an increase in (Da_H), (f) exhibits a slight rise. This is attributed to the enhanced permeability of the porous medium, which facilitates easier fluid flow along the fan's direction. As (Da_H) becomes larger, the y-component of the velocity vector

increases, while the x-component decreases. The variation of (f') in Fig. 4.4.1.2 also supports this observation. In Fig. 4.4.1.2 (f') exhibits a step increase with (Y) near the hot wall, indicating the boundary layer thickness where a sharp velocity gradient is present. Another steep gradient region is observed around (Y = 1), representing the upper part of the porous area where the flow is predominantly vertical, gradually transitioning as it approaches the heated surface.

As (Da_H) increases, the permeability of the porous medium improves, reducing flow resistance. This results in lower velocity gradients within the boundary layer, leading to a thicker boundary layer near the fan-driven flow's impingement, a trend visible in Fig. 4.4.1.2 Since the shear stress and frictional losses on the heated surface are influenced by the velocity gradient within the boundary layer, the shear stress decreases as (Da_H) increases. In Fig. 4.4.1.3, the variable (θ) decreases nearly exponentially with (Y), approaching zero. The region with a high gradient near the wall (Y = 0) represents the thermal boundary layer. As (Da_H) rises, the temperature gradient near the wall becomes steeper, leading to a reduction in the thermal boundary layer thickness. Based on Fick's law, the temperature gradient at the wall correlates with the heat flux. Consequently, higher heat transfer rates are expected with increasing (Da_H). This aligns with physical expectations, as a more permeable porous medium enhances (f') near the wall, thereby boosting convective heat transfer.

4.4.2 Study of the Reynolds number

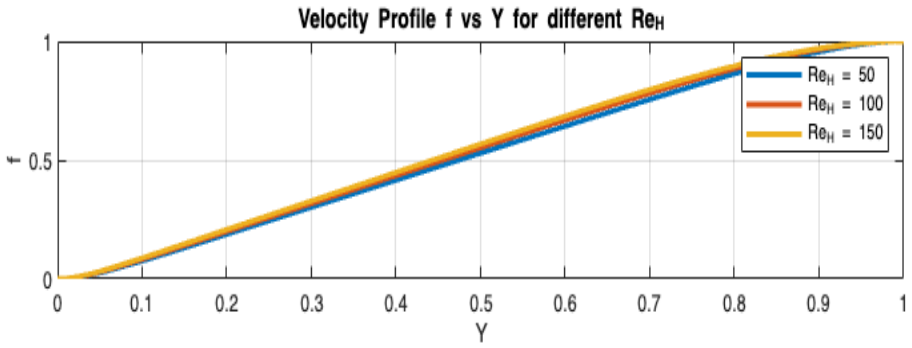

figure 4.4.2.1 Variation of f with respect to Re_H

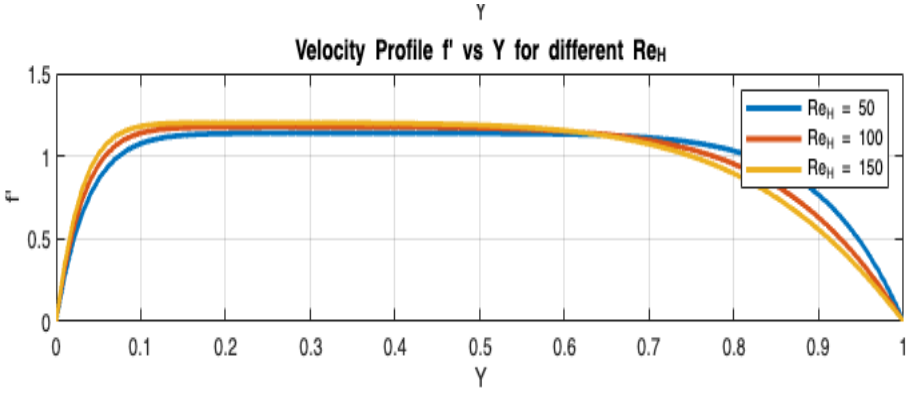

figure 4.4.2.2 Variation of f' with respect to Re_H

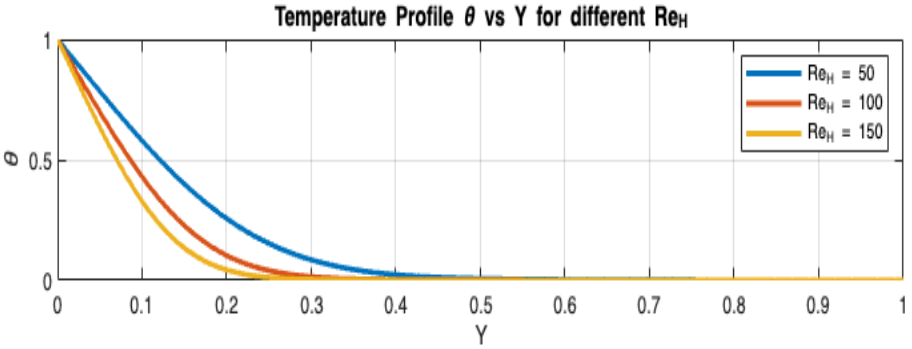

figure 4.4.2.3 Variation of θ with respect to Re_H

Figures 4.4.2.1, 4.4.2.2 and 4.4.2.3 illustrates how the distributions of f, f', and θ vary with the Reynolds number (Re_H) of the base fluid respectively. As Re_H rises, the momentum input of the fluid in the y-direction also increases, resulting in enhanced values of f. However, since the flow remains in the laminar, f does not exhibit significant sensitivity to changes in Re_H.

From Fig. 4.4.2.2, it is evident that increasing Re_H enhances the gradientof f′ close to the wall, whereas the slope diminishes at the upper part of the porous medium. As the fluid moves into the porous foam, it flows vertically at first, then transitions to horizontal flow due to the impingement on the surface. An increase in Re_H boosts the fluid's momentum, enabling it to maintain its initial flow state over a longer distance. Consequently, the slope of the velocity profile (f′) at the upper surface of the porous foam decreases with higher Re_H. In the laminar regime, an increase in Re_H results in a reduction of the boundary layer thickness. This causes a steeper gradient of f′ near the heated wall, leading to greater friction losses as Re_Hincreases.

Fig. 4.4.2.3 shows that increasing Re_H reduces the temperature distribution θ while increasing its gradient close to the heated wall. Same as the effect of the Darcy number Da_H, the rise in Re_H increases the heat transfer performance, contributing to higher thermal performance.

4.4.3 Hartmann number study

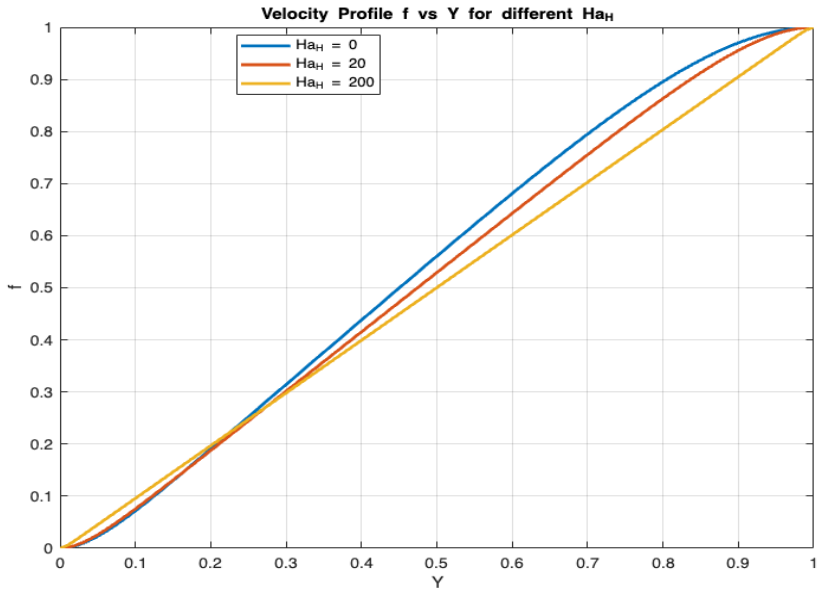

Figure 4.4.3.1 Variation of distribution of f with respect to Ha_H

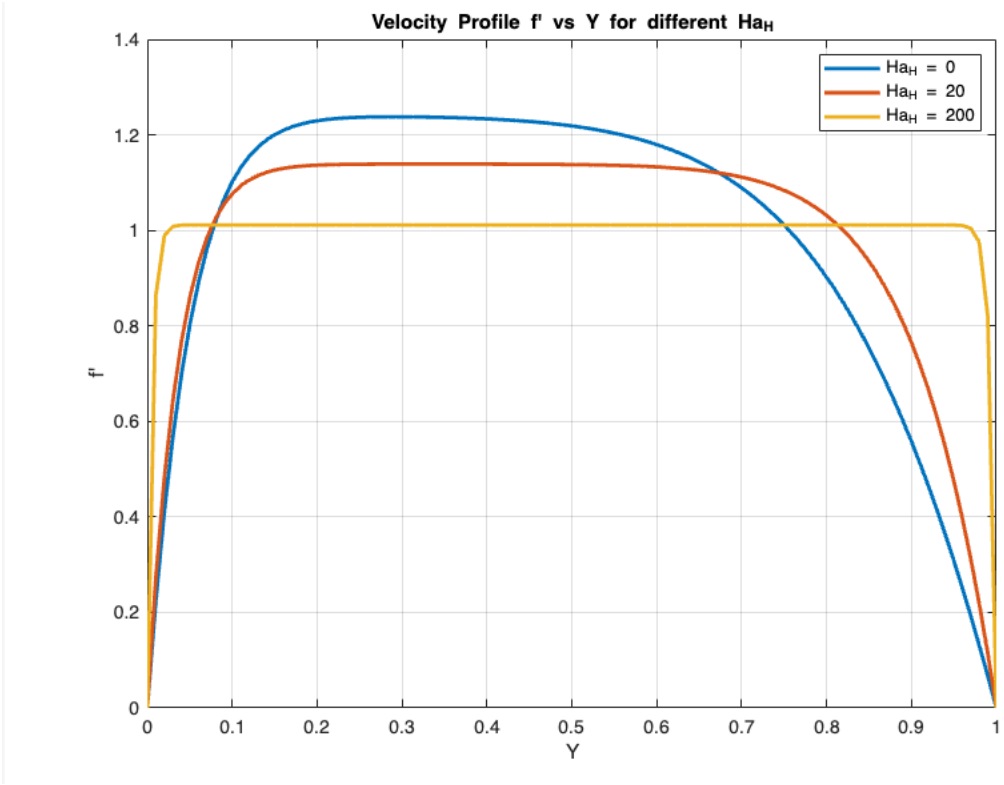

Figure 4.4.3.2 Variation of distribution of f' with respect to Ha_H

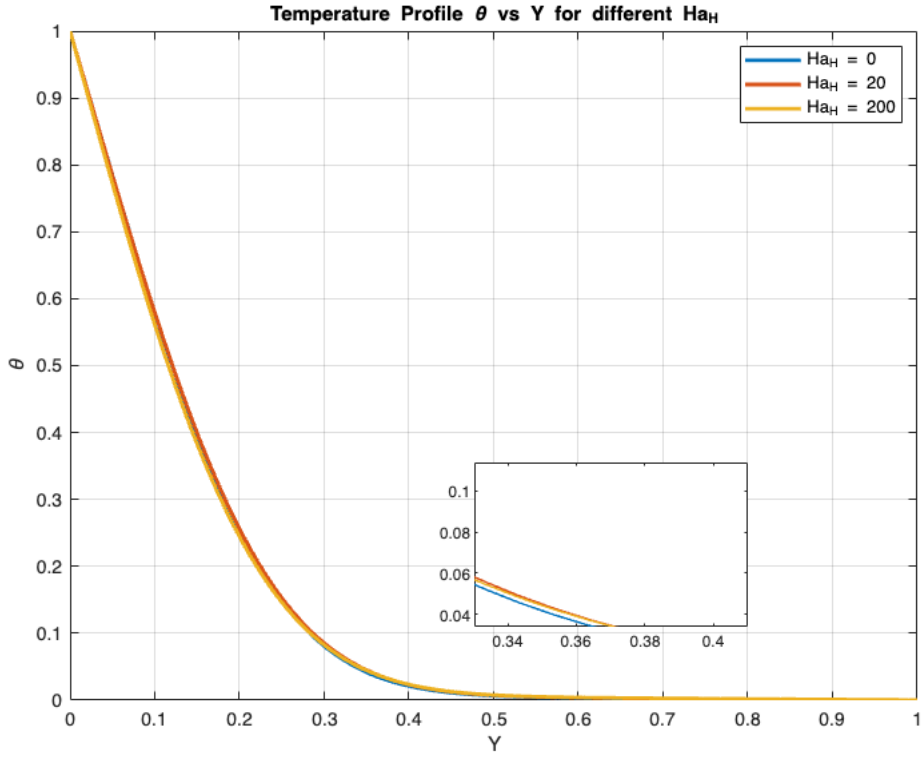

Figure 4.4.3.3 Variation of distribution of θ with respect to Ha_H

Figures 4.4.3.1, 4.4.3.2, and 4.4.3.3, illustrates the variations in the distributions of f, f′, and θ with respect to Ha_H for the base fluid respectively. According to Equation (3.7.2), increasing (Ha_H) for the base fluid enhances the magnetic body force, which operates in the x-direction and is directly proportional to the velocity (U). The magnetic force alters the direction of the impiging flow, changing it from vertical to horizontal. As seen in the figures above, as Ha_H increases, f decreases, and the f′ profile flattens. This suggests that as the vertical impingement flow enters the porous region, the magnetic force redirects it more horizontally. The stronger the magnetic field, the greater the rate of deflection, as evident from the behaviour in Fig. 4.4.3.2.

The horizontal magnetic force facilitates the transition of flow near the wall from a stationary state to the mainstream velocity. This action reduces the boundary layer thickness and increases the shear stress on the wall. Fig. 4.4.3.3 illustrates the effect of Ha_H on the temperature profile θ. It is evident that an increase in the Hartmann number (Ha_H) has a negligible effect on the temperature distribution, since the Hartmann number does not directly affect the energy equation (Equation 3.6.7). A more detailed analysis of the effects of Ha_H on heat transfer will be provided in Section 4.5.

4.5 Investigating effect of Hartmann number on Nusselt at different porosity

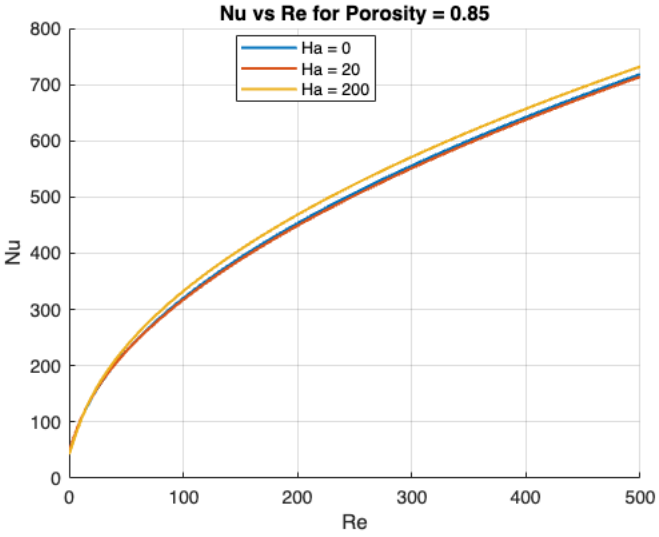

figure 4.5.1 Variation of Nusselt number and Reynolds number for 0.85 porosity

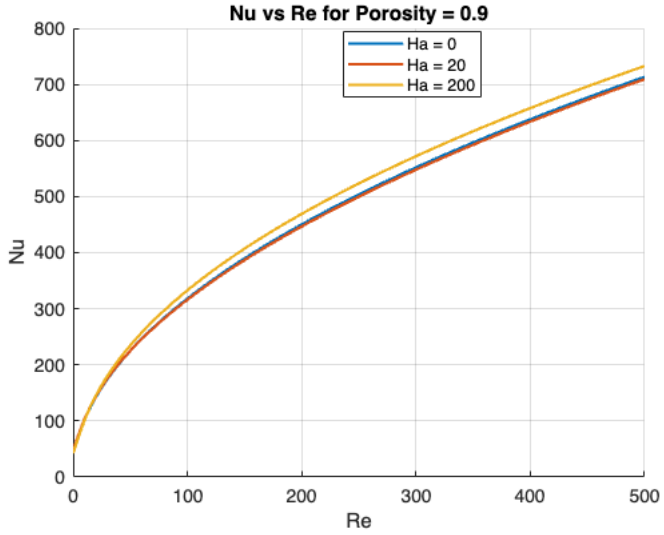

figure 4.5.2 Variation of Nusselt number and Reynolds number for 0.9 porosity

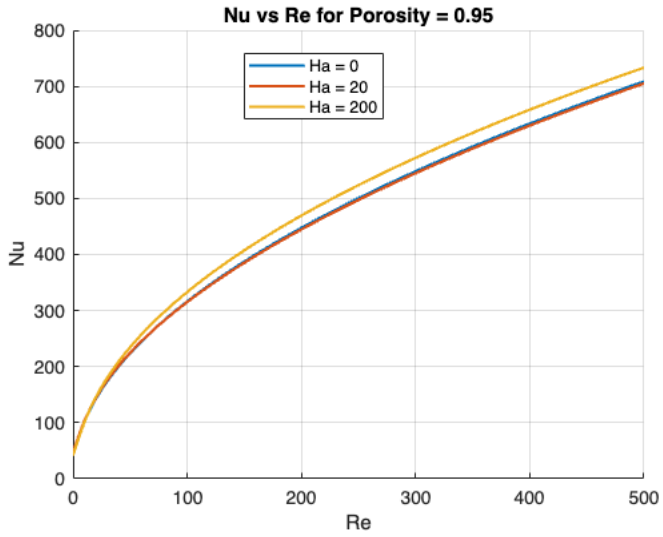

fugure 4.5.3 Variation of Nusselt number and Reynolds number for 0.95 porosity

The figures above illustrate how the Hartmann number (Ha_H) influences the Nusselt number (Nu) in relation to the Reynolds number across various porosities. It can be seen that as porosity rises, Nu diminishes. This reduction is due to the decline in effective thermal conductivity, which is influenced by the increase in Ha_H, as demonstrated in Equation (3.6.1). The thermal performance of the heat sink is affected by the magnetic field, and this effect changes depending on the porosity. For ϵ=0.85, an increase in Ha_H has almost no effect on Nu. However, for ϵ=0.95, increasing Ha_H results in a rise in Nu.

As explained in Section 4.4.3, increasing Ha_H enhances convective flow over the heated surface. Based on Eq. (3.6.7), a reduction in porosity enhances the impact of viscous dissipation on overall heat transfer. Since viscous dissipation negatively impacts heat transfer, at lower porosities, the enhanced convection because of the the magnetic force is counteracted by dissipation, reducing the heat transfer rate. At higher porosities, the impact of viscous dissipation decreases, leading to improved heat transfer due to the increase in Hartmann number (Ha_H).

CHAPTER 5

CONCLUSION AND RECOMMENDATION

5.1 CONCLUSION

This research analytically investigated the thermal performance of CNT-based nanofluids in PEG-400 under the influence of a magnetic field, with a focus on their application in cooling electronic devices. The focus is on enhancing heat transfer efficiency, optimizing the operating temperature range, and improving the overall reliability of thermal management systems in electronics. This study explores the behavior of CNT-PEG-400 nanofluids under the influence of a magnetic field. It focuses on key factors such as viscosity, density, heat transfer, and the impact of the Hartmann number.

In this study, we investigated the enhancement of flow through impingement cooling within a porous metal heat sink, utilizing CNT-PEG-400 nanofluids. The Darcy-Brinkman-Forchheimer framework is utilized to characterize the flow within porous media, incorporating viscous dissipation into the heat transfer equations. By applying appropriate similarity variables, the governing nonlinear partial differential equations are transformed into nonlinear ordinary differential equations, which are then solved through numerical methods.

This research demonstrated that parameters such as Reynolds number, Darcy number, Hartmann number, and porosity significantly influence flow behavior and heat transfer characteristics.The results from this parametric analysis are:

- CNTs increase the density and viscosity of PEG-400, contributing to better thermal performance.

- **Increasing Darcy number** enhances the profiles of the velocity and heat transfer, improving overall cooling performance.
- **Increasing the Hartmann number** reduces velocity profiles, leading to varying effects on heat transfer depending on porosity. For porosities beyond 0.9, a rise in Hartmann number results in an increase in Nusselt Number, thus, improving heat transfer performance.

These results contribute to optimizing cooling strategies for electronic devices, especially under the influence of magnetic fields, and highlight the significant role of porosity in determining the effectiveness of CNT-PEG-400 nanofluids in thermal management.

5.2 RECOMMENDATIONS

1. **Optimization of CNT Concentration**: Future work should explore the optimal concentration of carbon nanotubes (CNTs) in PEG-400 for different cooling scenarios. While CNTs enhance thermal conductivity, excessive concentrations may increase viscosity, which could negatively affect flow dynamics and energy consumption in the cooling system. An experimental or numerical investigation into the ideal CNT loading for maximizing heat transfer while minimizing adverse effects on fluid flow is recommended.

2. **Exploring Different Magnetic Field Strengths**: Since the Hartmann number (Ha) significantly influences heat transfer performance, especially in varying porosity conditions, further research should focus on optimizing the magnetic field strength for different cooling requirements. Experimental validation of these simulations with real-world electronic devices under different magnetic field strengths could help refine the findings and guide practical applications.

3. **Investigation of Other Base Fluids**: While PEG-400 has been used in this study as the cooling medium, future research could investigate other potential base fluids with

different thermophysical properties. This could include fluids with higher thermal conductivity or lower viscosity to determine if they provide better performance when combined with CNTs under a magnetic field.

APPENDIX

1. Darcy number study

```
% Parameters
Re_H = 50;  % Reynolds number
epsilon = 0.9;  % Porosity
c_E = 0.09;  % Constant
X = 1;  % Similarity variable
Ha_H = 20;  % Hartmann number
Pr = 0.71;  % Prandtl number
Ec = 0.001;  % Eckert number


% Range of Da_H values to test
Da_H_values = [5 * 10^(-4), 5 * 10^(-3), 5 * 10^(-2)];


% Spatial domain
Y = linspace(0, 1, 100);  % 100 points in the Y direction


% Store results for each Da_H value
f_results = zeros(length(Da_H_values), length(Y));
fp_results = zeros(length(Da_H_values), length(Y));
theta_results = zeros(length(Da_H_values), length(Y));


% Loop over Da_H values
for i = 1:length(Da_H_values)
    Da_H = Da_H_values(i);  % Current Da_H
```

```
    % Solve the momentum equation using bvp4c
    solinit = bvpinit(Y, @m_guess);  % Initial guess for momentum equation
    sol_f = bvp4c(@(x,y) momentum_ode(x, y, Re_H, epsilon, c_E, X, Da_H, Ha_H),
@momentum_bc, solinit);

    % Interpolating f, f', and f'' over Y
    f_interp = deval(sol_f, Y);     % f, f', f'' from momentum equation
    fp_interp = f_interp(2,:);  % f' is the second row
    fpp_interp = f_interp(3,:); % f'' is the third row

    % Store the results of f and f' for plotting later
    f_results(i, :) = f_interp(1,:);    % f
    fp_results(i, :) = fp_interp;       % f'

    % Solve the energy equation using bvp4c
    solinit_theta = bvpinit(Y, @theta_guess);  % Initial guess for energy equation
    sol_theta = bvp4c(@(x,y) energy_ode(x, y, f_interp, fp_interp, fpp_interp, Re_H, Pr, Ec, Da_H,
epsilon, X, Y), @energy_bc, solinit_theta);

    % Store the results for theta
    theta_results(i, :) = sol_theta.y(1,:);
end

% Plot f vs Y for different Da_H values
```

```
figure;
subplot(3, 1, 1);
for i = 1:length(Da_H_values)
    plot(Y, f_results(i, :), 'LineWidth', 2, 'DisplayName', ['Da_H = ', num2str(Da_H_values(i))]);
    hold on;
end
xlabel('Y');
ylabel('f');
title('Velocity Profile f vs Y for different Da_H');
legend show;
grid on;

% Plot f' vs Y for different Da_H values
subplot(3, 1, 2);
for i = 1:length(Da_H_values)
    plot(Y, fp_results(i, :), 'LineWidth', 2, 'DisplayName', ['Da_H = ', num2str(Da_H_values(i))]);
    hold on;
end
xlabel('Y');
ylabel('f''');
title('Velocity Profile f'' vs Y for different Da_H');
legend show;
grid on;

% Plot theta vs Y for different Da_H values
subplot(3, 1, 3);
for i = 1:length(Da_H_values)
```

```
    plot(Y, theta_results(i, :), 'LineWidth', 2, 'DisplayName', ['Da_H = ', num2str(Da_H_values(i))]);
    hold on;
end
xlabel('Y');
ylabel('\theta');
title('Temperature Profile \theta vs Y for different Da_H');
legend show;
grid on;
```

2. Reynolds number

```
% Parameters
Da_H = 5 * 10^(-3);  % Darcy number
epsilon = 0.9;  % Porosity
c_E = 0.09;  % Constant
X = 1;  % Similarity variable
Ha_H = 20;  % Hartmann number
Pr = 0.71;  % Prandtl number
Ec = 0.001;  % Eckert number

% Range of Re_H values to test
Re_H_values = [50, 100, 150];

% Spatial domain
Y = linspace(0, 1, 100);  % 100 points in the Y direction

% Store results for each Re_H value
```

```
f_results = zeros(length(Re_H_values), length(Y));
fp_results = zeros(length(Re_H_values), length(Y));
theta_results = zeros(length(Re_H_values), length(Y));


% Loop over Re_H values
for i = 1:length(Re_H_values)
    Re_H = Re_H_values(i);  % Current Re_H


    % Solve the momentum equation using bvp4c
    solinit = bvpinit(Y, @m_guess);  % Initial guess for momentum equation
    sol_f = bvp4c(@(x,y) momentum_ode(x, y, Re_H, epsilon, c_E, X, Da_H, Ha_H),
@momentum_bc, solinit);


    % Interpolating f, f', and f'' over Y
    f_interp = deval(sol_f, Y);     % f, f', f'' from momentum equation
    fp_interp = f_interp(2,:);  % f' is the second row
    fpp_interp = f_interp(3,:); % f'' is the third row


    % Store the results of f and f' for plotting later
    f_results(i, :) = f_interp(1,:);    % f
    fp_results(i, :) = fp_interp;       % f'


    % Solve the energy equation using bvp4c
    solinit_theta = bvpinit(Y, @theta_guess);  % Initial guess for energy equation
```

```
    sol_theta = bvp4c(@(x,y) energy_ode(x, y, f_interp, fp_interp, fpp_interp, Re_H, Pr, Ec, Da_H,
epsilon, X, Y), @energy_bc, solinit_theta);

    % Interpolate theta values over Y
    theta_interp = deval(sol_theta, Y);  % Interpolate to match Y points
    theta_results(i, :) = theta_interp(1,:);  % Store theta results
end

% Plot f vs Y for different Re_H values
figure;
subplot(3, 1, 1);
for i = 1:length(Re_H_values)
    plot(Y, f_results(i, :), 'LineWidth', 2, 'DisplayName', ['Re_H = ', num2str(Re_H_values(i))]);
    hold on;
end
xlabel('Y');
ylabel('f');
title('Velocity Profile f vs Y for different Re_H');
legend show;
grid on;

% Plot f' vs Y for different Re_H values
subplot(3, 1, 2);
for i = 1:length(Re_H_values)
    plot(Y, fp_results(i, :), 'LineWidth', 2, 'DisplayName', ['Re_H = ', num2str(Re_H_values(i))]);
    hold on;
```

```
end
xlabel('Y');
ylabel('f'');
title('Velocity Profile f'' vs Y for different Re_H');
legend show;
grid on;


% Plot theta vs Y for different Re_H values
subplot(3, 1, 3);
for i = 1:length(Re_H_values)
    plot(Y, theta_results(i, :), 'LineWidth', 2, 'DisplayName', ['Re_H = ', num2str(Re_H_values(i))]);
    hold on;
end
xlabel('Y');
ylabel('\theta');
title('Temperature Profile \theta vs Y for different Re_H');
legend show;
grid on;
```

3. Hartmann number study

```
% Parameters
Da_H = 5 * 10^(-3);  % Darcy number
epsilon = 0.9;  % Porosity
c_E = 0.09;  % Constant
X = 1;  % Similarity variable
Re_H = 50;  % Reynolds number
```

```
Pr = 0.71;  % Prandtl number
Ec = 0.001;  % Eckert number

% Range of Ha_H values to test
Ha_H_values = [0, 20, 200];

% Spatial domain
Y = linspace(0, 1, 100);  % 100 points in the Y direction

% Store results for each Ha_H value
f_results = zeros(length(Ha_H_values), length(Y));
fp_results = zeros(length(Ha_H_values), length(Y));
theta_results = zeros(length(Ha_H_values), length(Y));

% Loop over Ha_H values
for i = 1:length(Ha_H_values)
    Ha_H = Ha_H_values(i);  % Current Ha_H

    % Solve the momentum equation using bvp4c
    solinit = bvpinit(Y, @m_guess);  % Initial guess for momentum equation
    sol_f = bvp4c(@(x,y) momentum_ode(x, y, Re_H, epsilon, c_E, X, Da_H, Ha_H),
@momentum_bc, solinit);

    % Interpolating f, f', and f'' over Y
    f_interp = deval(sol_f, Y);     % f, f', f'' from momentum equation
    fp_interp = f_interp(2,:);  % f' is the second row
    fpp_interp = f_interp(3,:); % f'' is the third row
```

```
    % Store the results of f and f' for plotting later
    f_results(i, :) = f_interp(1,:);    % f
    fp_results(i, :) = fp_interp;       % f'

    % Solve the energy equation using bvp4c
    solinit_theta = bvpinit(Y, @theta_guess);  % Initial guess for energy equation
    sol_theta = bvp4c(@(x,y) energy_ode(x, y, f_interp, fp_interp, fpp_interp, Re_H, Pr, Ec, Da_H,
epsilon, X, Y), @energy_bc, solinit_theta);

    % Interpolate theta values over Y
    theta_interp = deval(sol_theta, Y);  % Interpolate to match Y points
    theta_results(i, :) = theta_interp(1,:);  % Store theta results
end

% Plot f vs Y for different Ha_H values
figure;
subplot(3, 1, 1);
for i = 1:length(Ha_H_values)
    plot(Y, f_results(i, :), 'LineWidth', 2, 'DisplayName', ['Ha_H = ', num2str(Ha_H_values(i))]);
    hold on;
end
xlabel('Y');
ylabel('f');
title('Velocity Profile f vs Y for different Ha_H');
legend show;
grid on;

% Plot f' vs Y for different Ha_H values
```

```
subplot(3, 1, 2);
for i = 1:length(Ha_H_values)
    plot(Y, fp_results(i, :), 'LineWidth', 2, 'DisplayName', ['Ha_H = ', num2str(Ha_H_values(i))]);
    hold on;
end
xlabel('Y');
ylabel('f"');
title('Velocity Profile f" vs Y for different Ha_H');
legend show;
grid on;

% Plot theta vs Y for different Ha_H values
subplot(3, 1, 3);
for i = 1:length(Ha_H_values)
    plot(Y, theta_results(i, :), 'LineWidth', 2, 'DisplayName', ['Ha_H = ', num2str(Ha_H_values(i))]);
    hold on;
end
xlabel('Y');
ylabel('\theta');
title('Temperature Profile \theta vs Y for different Ha_H');
legend show;
grid on;
```

4. effect of hartmann number on Nusselt for different porosities

```
% Constants
c_E = 0.09;
X = 1;
```

```
Pr = 0.71;
Ec = 0.001;
Da = 5e-3;
Re_range = linspace(0, 500, 100);  % Reynolds number from 0 to 500
Ha_values = [0, 20, 200];  % Hartmann numbers
porosities = [0.85, 0.9, 0.95];  % Different porosities

% Thermal conductivities
k_bf = 0.186;  % Base fluid thermal conductivity (PEG-400)
k_eff = 9.69386;  % Effective thermal conductivity (CNT-PEG-400)
H_L = 1;       % H/L ratio, given as 1

% Loop through each porosity value
for porosity_idx = 1:length(porosities)
    epsilon = porosities(porosity_idx);  % Porosity for current plot

    figure;  % Create a new figure for each porosity
    hold on;

    % Loop through each Hartmann number
    for Ha = Ha_values
        Nu = zeros(size(Re_range));  % Preallocate Nusselt number array

        % Loop through each Reynolds number
        for i = 1:length(Re_range)
            Re_H = Re_range(i);
            Da_H = Da / epsilon;
            Ha_H = Ha;
```

```
        % Initial guess for momentum equation
        solinit_momentum = bvpinit(linspace(0, 1, 100), @m_guess);

        % Solve momentum equation to get velocity profile f, f', f''
        sol_momentum = bvp4c(@(x, y) momentum_ode(x, y, Re_H, epsilon, c_E, X, Da_H, Ha_H),
...
                             @momentum_bc, solinit_momentum);
        Y = linspace(0, 1, 100);  % y-direction grid
        f = deval(sol_momentum, Y, 1);
        fp = deval(sol_momentum, Y, 2);
        fpp = deval(sol_momentum, Y, 3);

        % Initial guess for energy equation
        solinit_energy = bvpinit(linspace(0, 1, 100), @theta_guess);

        % Solve energy equation to get temperature profile θ, θ'
        sol_energy = bvp4c(@(x, y) energy_ode(x, y, f, fp, fpp, Re_H, Pr, Ec, Da_H, epsilon, X, Y),
...
                           @energy_bc, solinit_energy);
        theta_prime_0 = deval(sol_energy, 0, 2);  % Get θ'(0) value

        % Calculate Nusselt number based on the given relation
        Nu(i) = -(k_eff / k_bf) * (H_L)^(-1) * theta_prime_0;
    end

    % Plot Nu vs Re for the current Ha and epsilon
    plot(Re_range, Nu, 'DisplayName', ['Ha = ', num2str(Ha)]);
```

```
    end


    % Configure plot for current porosity
    xlabel('Re');
    ylabel('Nu');
    title(['Nu vs Re for Porosity = ', num2str(epsilon)]);
    legend('show');
    grid on;
    hold off;
end
```

5 Matlab Functions

Momentum_ode.m

```
function dydx = momentum_ode(x, y, Re_H, epsilon, c_E, X, Da_H, Ha_H)
    dydx = zeros(4,1);


    % y(1) = f, y(2) = f', y(3) = f'', y(4) = f'''
    dydx(1) = y(2);            % f' = y2
    dydx(2) = y(3);            % f'' = y3
    dydx(3) = y(4);            % f''' = y4
    dydx(4) = -(Re_H / epsilon) * y(1) * y(4) + ...
            (2 * c_E * epsilon * X * Re_H / sqrt(Da_H) + Re_H / epsilon) * y(2) * y(3) + ...
            epsilon * (1 / Da_H + Ha_H^2) * y(3);
end
```

momentum_bc.m

```
function res = momentum_bc(ya, yb)
    res = [ya(1);  % f(0) = 0
          ya(2);  % f'(0) = 0
          yb(1) - 1;  % f(1) = 1
```

```
        yb(2)];     % f'(1) = 0
end
```

m_guess.m

```
function g = m_guess(x)
    g = [x; 0; 0; 0];  % Guess for [f, f', f'', f''']
end
```

energy_ode.m

```
function dydx = energy_ode(x, y, f_interp, fp_interp, fpp_interp, Re_H, Pr, Ec, Da_H, epsilon, X, Y)
    % Interpolate the values of f, f', and f'' at the current position x
    f = interp1(Y, f_interp(1,:), x);      % f(x)
    f_prime = interp1(Y, fp_interp, x);    % f'(x)
    f_double_prime = interp1(Y, fpp_interp, x);  % f''(x)

    % Energy equation ODE system
    dydx = zeros(2,1);
    dydx(1) = y(2);  % θ'
    % Main energy equation with convective and conductive terms
    dydx(2) = -Pr * Re_H * f * y(2) - Pr * Ec * (1/Da_H * (X^2 * f_prime^2 + f^2) + 1/epsilon * (4 *
f_prime^2 + X^2 * f_double_prime^2));
end
```

energy_bc.m

```
function res = energy_bc(ya, yb)
    res = [ya(1) - 1;   % theta(0) = 1
        yb(1)];      % theta(1) = 0
end
```

theta_guess.m

```
function g = theta_guess(x)
    g = [1 - x; 0];  % Guess for [theta, theta']
```

```
end
```

REFERENCES

1. Abdelaziz, G. B., Abdelaziz, M. G., Ahmed, S. E., & Alshomrani, A. S. (2024). Numerical study of heat transfer enhancement by applying magnetic field on nanofluid flowing in porous medium. *Arabian Journal for Science and Engineering*, 49, 15497–15508. https://doi.org/10.1007/s13369-024-09106-2

2. ACS Omega Team. (2024). Review on Nanofluids: Preparation, Properties, Stability, and Thermophysical Characteristics. *ACS Omega*, 9. https://doi.org/10.1021/acsomega.4c03279

3. Adio, S. A., Atofarati, E. O., Muritala, A. O., Huan, Z., & Veeredhi, V. R. (2025). Nanofluids flow boiling and convective heat transfer in microchannels: a systematic review and bibliometric analysis. *Journal of Thermal Analysis and Calorimetry*, 22 May 2025. https://doi.org/10.1007/s10973-025-14265-x

4. Ahmadi, G., Toghraie, D., Sedighi, K., & Karimipour, A. (2018). A review on nanofluids: Preparation, stability mechanisms, thermal conductivity, and applications. *Journal of Molecular Liquids*, 266, 420-437. doi:10.1016/j.molliq.2018.06.106

5. Calmidi, V. V., & Mahajan, R. L. (2000). Forced convection in high porosity metal foams. *J. Heat Transfer*, *122*(3), 557-565.
6. Cwynar, K., Dziadosz, J., Scheller, Ł., Zorębski, E., Jędrysiak, R., Kolanowska, A., ... & Dzida, M. (2023). On isobaric heat capacity of ionanofluids with carbon nanotubes–An experimental study. *Journal of Molecular Liquids*, *387*, 122535.

7. Dhinesh Kumar, R., & Suresh, S. (2021). Magnetic field-induced thermal convection of nanofluids in geothermal applications. *Geofluids*, 2021, 3209855.

8. Feng, S. S., Kuang, J. J., Lu, T. J., & Ichimiya, K. (2015). Heat transfer and pressure drop characteristics of finned metal foam heat sinks under uniform impinging flow. *Journal of Electronic Packaging*, *137*(2), 021014.
9. Jang, B. K., Sakka, Y., & Woo, S. K. (2009, March). Alignment of carbon nanotubes by magnetic fields and aqueous dispersion. In *Journal of Physics: Conference Series* (Vol. 156, No. 1, p. 012005). IOP Publishing.

10. Li, W., Hu, L., Jiang, C., & Li, W. (2020). Preparation, characterization and application of carbon nanotube based nanofluids. *Renewable and Sustainable Energy Reviews*, 117, 109466.

11. Li, X., Tu, Y., Zhao, Y., Hu, X., Liu, B., & Huang, Y. (2018). Synthesis of carbon nanotubes by catalytic chemical vapor deposition using a single precursor: acetylene. *Materials Research Express*, 5(5), 055602.

12. Lou, D., Grablander, T., Mao, M., Hong, H., & Peterson, G. P. (2021). Improved thermal conductivity of PEG-based fluids using hydrogen bonding and long chain of nanoparticle. *Journal of Nanoparticle Research*, *23*, 1-10.

13. Mahian, O., Kolsi, L., Amani, M., Estellé, P., Ahmadi, G., Kleinstreuer, C., ... & Pop, I. (2019). Recent advances in modeling and simulation of nanofluid flows-Part I: Fundamentals and theory. *Physics reports*, *790*, 1-48.

14. Marcos, M. A., Podolsky, N. E., Cabaleiro, D., Lugo, L., Zakharov, A. O., Postnov, V. N., ... & Semenov, K. N. (2019). MWCNT in PEG-400 nanofluids for thermal applications: A chemical, physical and thermal approach. *Journal of Molecular Liquids*, *294*, 111616.
15. Nabwey, H. A., Armaghani, T., Azizimehr, B., Rashad, A. M., & Chamkha, A. J. (2023). A comprehensive review of nanofluid heat transfer in porous media. *Nanomaterials*, 13(5), 937. https://doi.org/10.3390/nano13050937
16. Narang, J. and Pundir, C.S. (2018) Current and future developments in nanomaterials and carbon nanotubes. volume 1, Introduction to Carbon Nanomaterials. *Sharjah, UAE: Bentham Science Publishers*.
17. Pourrahmani, H., Moghimi, M., Siavashi, M., & Shirbani, M. (2019). Sensitivity analysis and performance evaluation of the PEMFC using wave-like porous ribs. *Applied Thermal Engineering*, *150*, 433-444.
18. Punia, A., & Ray, R. K. (2024). New Higher-Order Super-Compact Scheme for Enhanced Three-Dimensional Heat Transfer with Nanofluid and Conducting Fins. *arXiv:2411.09818*
19. Sarkar, S. (2019). Nanofluids: Fundamentals, Properties and Applications. Wiley.

20. Shampine, L. F., Gladwell, I., & Thompson, S. (2003). Solving ODEs with matlab. *Cambridge university press*.
21. Sigma-Aldrich. (n.d.). Polyethylene glycol 400. Material Safety Data Sheet. Retrieved from https://www.sigmaaldrich.com

22. Sudhakar, N., & Ravi Kumar, P. V. (2014). The Behavior of Nano-Fluids Under the Influence of Magnetic Field. *International Journal of Advanced Research in Electrical, Electronics and Instrumentation Engineering*, 3(3), 10783-10793.

23. Vafai, K. (Ed.) (2023). The Role of Nanofluids in Renewable Energy Engineering. *Springer*. ISBN 978-3036593821

24. Venkateswarlu B., Chavan S., Joo W. S., Kim C. S. (2024). A numerical simulation of heat transfer performance of MHD nanofluids in porous metal for enhancing CPU cooling efficiency. *Waves in Random and Complex Media*, 1-27.

25. Wang, B., Zhang, Y., Li, X., Liu, H., & Zhao, J. (2019). Experimental study on heat transfer characteristics of carbon nanotube nanofluids under a magnetic field. *Applied Sciences*, 9(7), 1409.

26. Whelan, B. P., Kempers, R., & Robinson, A. J. (2012). A liquid-based system for CPU cooling implementing a jet array impingement waterblock and a tube array remote heat exchanger. *Applied Thermal Engineering*, *39*, 86-94.

27. Xie, H., Chen, L., Wang, J., Shen, X., & Yang, Y. (2018). Experimental study on the viscosity of carbon nanotube aqueous nanofluids under magnetic field. *Nanomaterials*, 8(6), 393.

28. Yin, Q., Sun, K. N., Li, A. J., Shao, L., Liu, S. M., & Sun, C. (2008). Study on carbon nanotube reinforced phenol formaldehyde resin/graphite composite for bipolar plate. *Journal of power sources*, *175*(2), 861-865.

29. Younes, H., Mao, M., Murshed, S. S., Lou, D., Hong, H., & Peterson, G. P. (2022). Nanofluids: Key parameters to enhance thermal conductivity and its applications. *Applied Thermal Engineering*, *207*, 118202.

30. Yu, W., Liu, C. & Fan, S. Advances of CNT-based systems in thermal management. *Nano Res.* **14**, 2471–2490 (2021). https://doi.org/10.1007/s12274-020-3255-1

31. Zamir, S., & Hayat, T. (2024). Induced magnetic field characteristics on time-dependent MHD Casson nanofluid over an inclined stretchable sheet. *Nanothermodynamics Review*. https://doi.org/10.1515/ntrev-2024-0117

32. Zing, C., Mahjoob, S., & Vafai, K. (2019). Analysis of porous filled heat exchangers for electronic cooling. *International Journal of Heat and Mass Transfer*, *133*, 268-276.